We are IntechOpen, the world's leading publisher of Open Access books Built by scientists, for scientists

6,900
Open access books available

185,000
International authors and editors

200M
Downloads

Our authors are among the

154
Countries delivered to

TOP 1%
most cited scientists

12.2%
Contributors from top 500 universities



WEB OF SCIENCE™

Selection of our books indexed in the Book Citation Index in Web of Science™ Core Collection (BKCI)

Interested in publishing with us?
Contact book.department@intechopen.com

Numbers displayed above are based on latest data collected.
For more information visit www.intechopen.com



Chapter

Chattering-Free Robust Adaptive Sliding Mode Speed Control for Switched Reluctance Motor

Mohammad Masoud Namazi, Hamid Reza Koofigar and Jin-Woo Ahn

Abstract

This study describes an adaptive sliding mode control (ASMC) for the control of switched reluctance motor (SRM). The main objective is to minimize torque ripples with controller effort smoothness while the system is under perturbation by structured uncertainties, unknown parameters, and external disturbances. The control algorithm employs an adaptive approach to remove the need for prior knowledge within the bound of perturbations. This is suitable for tackling the chattering problem in the sliding motion of ASMC. In order to achieve control effort smoothness and more effective elimination of chattering, the algorithm then incorporates proper modifications in order to build a chattering-free robust adaptive sliding mode control (RASMC) using Lyapunov stability theory. A final advantage of the algorithm is that system stability and error convergence are guaranteed. The effectiveness of the proposed controller in improving robustness and minimizing ripples is demonstrated by numerical simulation. Experimental validation is used to demonstrate the efficiency of the proposed scheme. The results indicate that RASMC provides a superior performance with respect to speed tracking and disturbance rejection over the conventional sliding mode control (CASMC) in the face of uncertainties in model and dynamic loads.

Keywords: switched reluctance motor, ripple minimization, robust adaptive sliding mode control, chattering elimination, automotive application

1. Introduction

The past two decades witnessed a unique interest in using switched reluctance motors fueled by their several advantages over other motors. Therefore, one can expect them to play a more crucial role in the industry in the future. The rotor of switched reluctance motor (SRM) has no winding, which gives more preference to the machine, including smaller size, lower costs, higher speeds, and high-power density and reliability [1].

Double saliency structure, inherent magnetic saturation, and time variation of parameters induce nonlinear complexity and high uncertainties in the dynamic model. Furthermore, the load torque uncertainties in many applications such as

variable payloads are inevitable. One biggest challenge in SRM drives is torque ripples. Therefore, compared with other methods like magnetic structure design to achieve minimized torque ripple performance, advanced control methods have been considered further, including model predictive control [2], fuzzy logic controller [3], internal model control [4], Lyapunov function-based robust controller [5], and H-infinity robust technique [6, 7]. Moreover, applications of nonlinear robust adaptive algorithms for SRM control have been proposed in [8, 9]. However, the sophisticated design of these methods is their disadvantage. Hence, appropriate simple nonlinear control design regarding uncertainties is necessary.

Recently, designing controllers based on variable structure system and sliding mode control (SMC) thanks to its features such as simplicity, high-speed feedback control that could be easily used along with motor switching circuit, and inherent robustness against nonlinear complex uncertain dynamic systems has been the focus of many researchers. Conventional SMC (CSMC) design for torque control considering ripple reduction is used in [10–14], but these methods unfortunately suffer from the chattering phenomenon. To solve this problem, several attempts are reported for SRM control that is briefly mentioned as follows.

Ref. [15] introduced robust variable structure control causing reduced torque ripple operation. However, the magnetic saturation is neglected. Ref. [16] proposed SMC-based flux linkage controller for switched reluctance motor. Advantage of chattering reduction is achieved by using boundary layer around the switch surface. However, this method creates a finite steady-state error [17]. The idea of using continuous sliding mode function is also presented in [18]. Fuzzy discontinuous SMC for this purpose is developed in [19], but the results show that chattering exists. Ref. [20] uses a dynamic sliding mode controller in the input of the speed controller instead of sign function, but external disturbance and system uncertainties are not considered. Ref. [21] developed chattering-free nonlinear sliding mode controller; however, it focused on permanent magnet synchronous motor. Higher order sliding mode control (HOSMC) is also proposed for alleviating the chattering problem [22, 23]. For example, [24] proposed second-order sliding mode control (SOSM) with super-twisting algorithm for speed control of SRM but unfortunately it only contains simulation results. Application of second-order sliding mode control with the focus on dynamic improvement of phase currents is also proposed in [25].

The deficiency of most designed controllers based on sliding mode is a result of the requirement of prior knowledge about upper bound of uncertainties and unmodeled dynamics. In other words, the regular SMC estimates upper bound of perturbations through calculation of switching gain to compensate their undesired effect. The gain increases with higher value of upper bound and leads to chattering phenomenon and control effort intensification. This may excite high frequency, which causes problems for hardware implementing. Chattering-free approaches for design SMC are classified in two major categories: interaction with switching gain selection and dynamic modification in sliding function [26]. In the case of switching gain selection, one useful approach is adaptive-based sliding mode controls (ASMC) [27, 28].

In this paper, it is further attempted to develop a SRM drive speed control aiming to torque ripple minimization. In doing so, a robust adaptive-based scheme was applied to overcome the uncertainties of model and load torque. The main idea lies in estimation of desired switching gain to reduce chattering. To make this, there is no need to know the upper bound of uncertainties. On the other hand, control gain is tried to be maintained as small as possible that is sufficient to counteract the uncertainties. The method is used successfully in AC electric drive [29, 30].

In recent years, there is a growing concern to integrate the chattering reduction techniques for building a unified effective method to yield chattering-free

performance. For example, [31, 32] integrate HOSMC with gain adaptation techniques. RASMC, which replaces discontinuous sign function by continuous tanh function with incorporation of ASMC, is introduced in [33, 34]. Reference [35] proposed modified robust adaptive control, while the modification occurred in error dynamic definition not in switching function.

A robust adaptive controller by incorporating exponential function instead of discontinuous function is proposed in [36, 37]. Some changes are applied to the control law so that signals of closed-loop system would finally become uniformly bounded. This method is effective in reducing and smoothing the control effort by developing simple estimation of sliding gain despite unknown time-varying perturbations. The approach benefits from the low computational process.

This paper tries to employ RASMC for chattering-free speed control of SRM with high-accuracy robust tracking performance under structured uncertainties and perturbations. The proposed scheme can reject any applied unknown bounded, time-varying disturbances. Torque ripple minimization and transient response improvement are also tried to be achieved. Additionally, the presented method demonstrates control effort considerable smoothness. Asymptotic stability is retained by Lyapunov theory, and it is shown that states of the closed-loop system are bounded and asymptotically converge on zero. The validity and effectiveness of the proposed algorithm have been demonstrated by simulation and experiment. The implementation is presented using a 4KW, four-phase, DSP-based SRM drive system. The results verify the desired performance of proposed strategy by comparing with CASMC.

2. The dynamic model of SRM

The SRM possesses a simple design with salient poles on both the rotor and stator but without windings on its rotor. Operation is based on the tendency to stand in alignment with the rotor and stator poles which yields a stable position, and consequently, the reluctance is minimized. Torque production is due to the sequential excitation of diametrically opposite stator poles by a switching algorithm [25]. The basic sets of electrical and mechanical differential equations are used for dynamic modeling of SRM. The motor state–space dynamic model can be stated as

$$\begin{aligned} \dot{\theta} &= \omega, \\ J\dot{\omega} &= T_{\mathrm{e}} - T_{\mathrm{L}} - B\omega, \\ v &= ri + \frac{d\lambda(\theta, i)}{dt} \end{aligned} \tag{1}$$

where v is the voltage, i denotes the current, λ is the flux linkage, and r stands for the phase resistance. Moreover, J is the inertia of the motor, B denotes the motor load friction, T_{e} is the electromagnetic torque, and T_{L} shows the load torque.

3. Conventional adaptive sliding mode control design

In the conventional SMC, the upper bound of uncertainties is needed in controller design, whereas adaptive sliding mode method may estimate the bound of perturbations. By taking the uncertainties into account in the mechanical part of SRM dynamic model (1), one can write

$$\dot{\omega} = (a + \Delta a)\omega + (b + \Delta b)(T_e - T_{\mathrm{L}}) \tag{2}$$

where $a = -B/J$ and $b = 1/J$ denote the nominal parameters and Δa and Δb are unknown parts. Defining the speed error as $e = \omega_{ref} - \omega$, where ω_{ref} is a reference speed, the sliding surface may be adopted as $S = \sigma e + \dot{e}$, $\sigma > 0$. Therefore,

$$\dot{S} = \sigma\dot{e} + \ddot{e} = \sigma\left(\dot{\omega}_{ref} - \dot{\omega}\right) + \left(\ddot{\omega}_{ref} - \ddot{\omega}\right) = \sigma\left(-\dot{\omega}\right) - \ddot{\omega} \tag{3}$$

Substituting the derivative of $\dot{\omega}$ from (1) into (3), one obtains

$$\dot{S} = \sigma(-\dot{\omega}) - \left(\frac{B}{J}\dot{\omega} + \frac{1}{J}\left(\dot{T}_e - \dot{T}_L\right)\right) = \sigma(-\dot{\omega}) - \left(a\dot{\omega} + b\left(\dot{T}_e - \dot{T}_L\right)\right) \tag{4}$$

Incorporating the uncertainties in (4) yields

$$\begin{aligned} \dot{S} &= \sigma(-\dot{\omega}) - (a + \Delta a)\dot{\omega} - (b + \Delta b)\left(\dot{T}_e - \dot{T}_L\right) \\ &= -(\sigma + a)\dot{\omega} - b\dot{T}_e + b\dot{T}_L - b\left[\frac{1}{b}\left(\dot{\omega}\Delta a + \Delta b\left(\dot{T}_e - \dot{T}_L\right)\right)\right] \end{aligned} \tag{5}$$

By defining $P = \frac{1}{b}\left(\dot{\omega}\Delta a + \Delta b\left(\dot{T}_e - \dot{T}_L\right)\right)$ as the lumped uncertainty, the sliding dynamic (5) can be rewritten as

$$\dot{S} = -(\sigma + a)\dot{\omega} - b\dot{T}_e + b\dot{T}_L - bP \tag{6}$$

The instantaneous torque $T_e(\theta, i)$ can be expressed as

$$T_{\mathrm{e}}(\theta, i) = \frac{1}{2}i^2\frac{\mathrm{d}L(\theta)}{\mathrm{d}\theta} \rightarrow T_{\mathrm{e}}(\theta, i) = \frac{1}{2}\frac{L_a - L_u}{\theta_2 - \theta_1}i^2 = \frac{1}{2}Ci^2 \rightarrow \dot{T}_{\mathrm{e}} = Cidi \rightarrow \dot{T}_{\mathrm{e}} \propto i = u$$

where L_u is the inductance at unaligned position, L_a is the inductance at aligned position, and constant C is the slope of the inductance corresponding to rotor position [26]. The approximated inductance profile of the SRM, by neglecting magnetic saturation, is shown in **Figure 1**. Thus, the dynamic Eq. (6) can be written as

$$\dot{S} = -(\sigma + a)\dot{\omega} - bu + b\dot{T}_L - bP \tag{7}$$

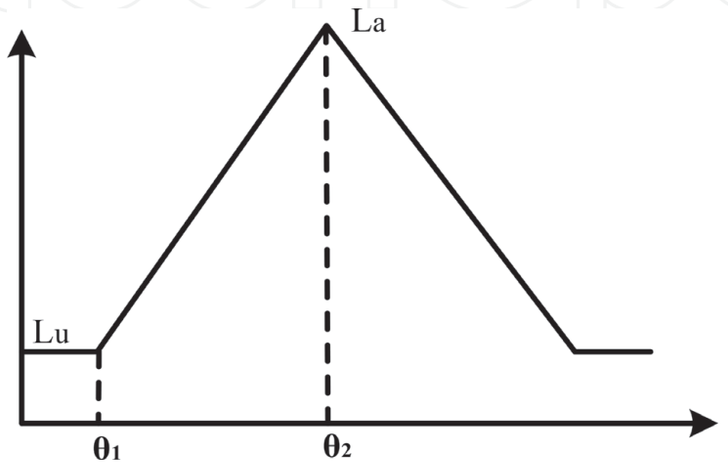


Figure 1.
Linear inductance profile of SRM [25].

Now, define the Lyapunov function candidate

$$V = \frac{1}{2}S^2 + \frac{1}{2\rho}\tilde{P}^2 \tag{8}$$

in which ρ is a positive constant and $\tilde{P} = P - \hat{P}$ is the error between the actual value of the lumped uncertainty P and its estimated value $\hat{P}$. The derivative of (8) is obtained as (the detailed manipulations are given in Appendix A)

$$\dot{V} = -K_1S^2 + S\left[-(\sigma + a)\dot{\omega} - b\left(u + \hat{P}\right) + b\dot{T}_L + K_1S\right] - \tilde{P}\left(\frac{1}{\rho}\dot{\hat{P}} + bS\right) \tag{9}$$

where K_1 is a positive constant. By choosing the control input u as

$$u = \frac{1}{b}\left[-(\sigma + a)\dot{\omega} - b\hat{P} + b\dot{T}_L + K_1S\right] \tag{10}$$

and substitution in (9), one can obtain

$$\dot{V} = -K_1S^2 - \tilde{P}\left(\frac{1}{\rho}\dot{\hat{P}} + bS\right) \tag{11}$$

Hence, adopting the adaptation law

$$\dot{\hat{P}} = -\rho bS \tag{12}$$

in (11) gives

$$\dot{V}_2 = -K_1S^2 \leq 0 \tag{13}$$

and the speed error $e \to 0$ as $t \to \infty$ can be concluded, by using the Lyapunov stability theorem [22, 27].

4. The proposed robust adaptive speed control for SRM

The previous section focused on using an adaptive scheme to estimate the upper bound of model uncertainties. However, the linear model of SRM is used, and only the mechanical uncertainties are considered.

This section proposes an effective solution for eliminating chattering by introducing the RASMC, with incorporating the exponential functions as an effective strategy to smoothen the control effort and reduce chattering. This algorithm is introduced to overcome both the mechanical and electrical uncertainties in the SRM model and the time-varying load torque disturbances. The upper bound of uncertainties is not required in the design procedure and is estimated by an adaptation mechanism to make the control gain small enough. The current dynamics can be written as [28]

$$\frac{di_j}{dt} = \left(\frac{\partial\lambda_j(\theta, i_j)}{\partial i_j}\right)^{-1}\left\{-ri_j - \frac{\partial\lambda_j(\theta, i_j)}{\partial\theta}\omega + v_j\right\} \tag{14}$$

where $j = 1, 2, 3, 4$ stands for each phases of the machine. The SRM dynamic model can be described in an affine form as [28]

$$\begin{aligned} \dot{x}_1 &= x_2, \\ \dot{x}_2 &= f(\mathbf{x}, t) + g(\mathbf{x}, t)u \end{aligned} \tag{15}$$

where $\mathbf{x} = [x_1 \;\; x_2]^T = [\omega \quad \dot{\omega}]^T$ and u, respectively, represent the state vector and control input. Defining $y = x_1 = \omega$ as the output, the dynamic model can be represented in the second-order compact affine form

$$\ddot{y} = f(\mathbf{x}, t) + g(\mathbf{x}, t)u \tag{16}$$

where the nonlinear functions $f(\mathbf{x}, t)$ and $g(\mathbf{x}, t)$ are specified by [18, 29]

$$\begin{aligned} f(\mathbf{x}, t) = \frac{1}{J}\Bigg\{ & \sum_{j=1}^{4}\left(\frac{\partial T_{ej}(\theta, i_j)}{\partial i_j}\right)\left(\frac{\partial \lambda_j(\theta, i_j)}{\partial i_j}\right)^{-1}\left(-r i_j - \frac{\partial \lambda_j(\theta, i_j)}{\partial \theta}\omega\right) \\ & + \omega \sum_{j=1}^{4}\left(\frac{\partial T_{ej}(\theta, i_j)}{\partial \theta}\right) - B\dot{\omega}\Bigg\} - \frac{T_u(t)}{J} \\ g(\mathbf{x}, t) = \frac{1}{J}\left(\frac{\partial T_{ej}(\theta, i_j)}{\partial i_j}\right)\left(\frac{\partial \lambda_j(\theta, i_j)}{\partial i_j}\right)^{-1} & \end{aligned} \tag{17}$$

in which $T_u(t)$ denotes the rate of variations in load torque, assumed here as a time-varying disturbance with unknown bound. In (17), the partial derivatives of flux and torque with respect to current and position are calculated by using the electromagnetic characteristics, achieved by the finite element method and verified

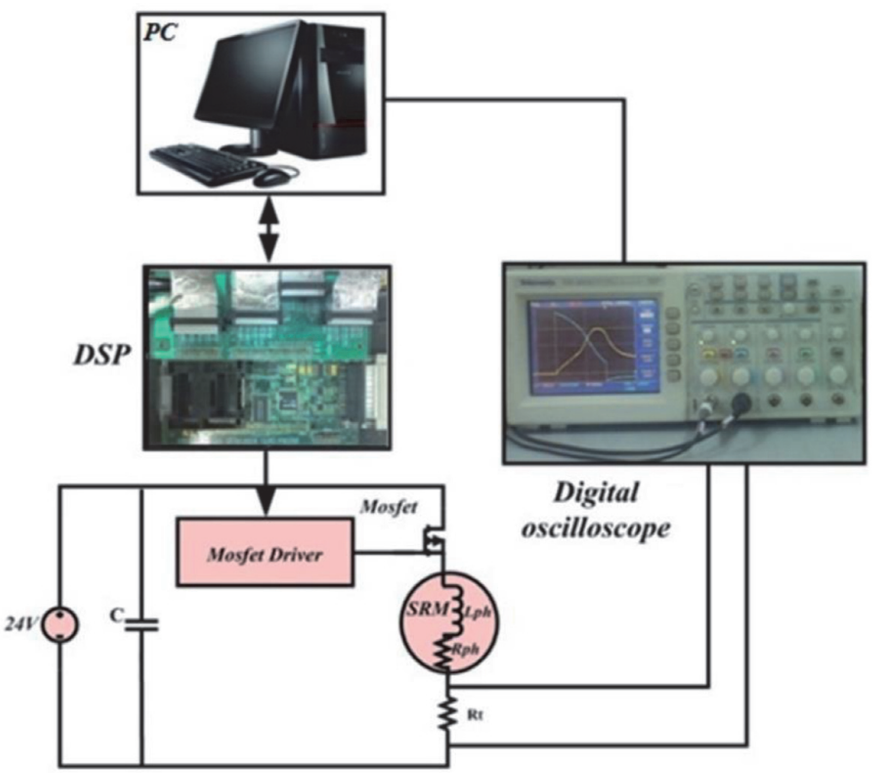


Figure 2.
Data measuring experimental layout.

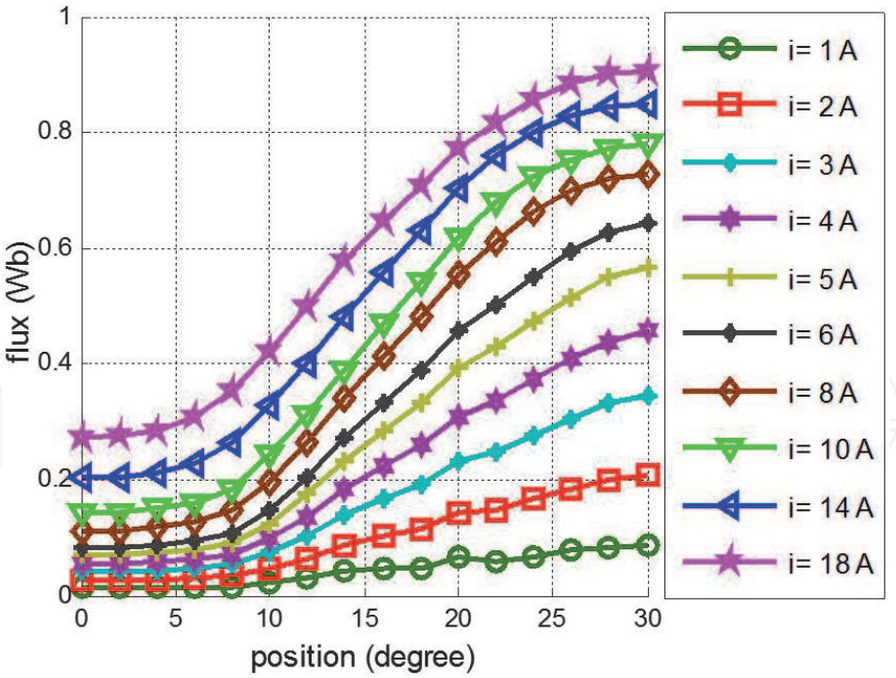


Figure 3.
Flux linkage vs. current vs. rotor position characteristics of prototype 8/6 SRM.

by experimental measurement. The layout of experimental test setup and the measured flux linkage curves are shown in **Figures 2** and **3**.

As a preliminary step to design procedure, rewrite (16) despite the time-varying external disturbance $d(t)$ as

$$\ddot{y} = f(\mathbf{x},t) + g(\mathbf{x},t)\,u + d(t) \tag{18}$$

The uncertain nonlinear term $f(\mathbf{x},t)$ is decomposed as [29]

$$f(\mathbf{x},t) = f_0(\mathbf{x},t) + \Delta f(\mathbf{x},t) \tag{19}$$

where $f_0(\mathbf{x},t)$ is the known part and $\Delta f(\mathbf{x},t)$ represents the model uncertainty with unknown bound. By augmenting the unknown uncertainty $\Delta f(\mathbf{x},t)$ and the external disturbance $d(t)$, an unknown time-varying uncertainty is defined as

$$h(t) = \Delta f(\mathbf{x},t) + d(t) \tag{20}$$

Hence, the SRM nonlinear dynamic model (18) takes the form

$$\ddot{y} = f_0(\mathbf{x},t) + g(\mathbf{x},t)u + h(t) \tag{21}$$

The goal is to design a controller that adaptively tunes the controller gain while all the closed-loop signals are bounded.

Assumption 1. The time-varying augmented parameter $h(t)$ is bounded by the unknown parameter $\alpha > 0$, i.e., $\|h(t)\| \le \alpha$.

Assumption 2. Without loss of generality, assume $g(\mathbf{x},t) > 0$, to derive the control law. However, this assumption is always satisfied for SRM, as the expressions $\partial\lambda(\theta,i)/\partial i$ and $\partial \mathrm{T}(\theta,i)/\partial i$ are shown to be positive.

Considering $\lambda(\theta,i) = \mathrm{L}(\theta,i)\,i$ one obtains

$$\frac{\partial \lambda(\theta,i)}{\partial i} = L(\theta,i) + i\frac{\partial L(\theta,i)}{\partial i} \tag{22}$$

From a physical viewpoint, it is true to assume the positivity of (22) in the range of operation [10], i.e.,

$$L(\theta,i)+i\frac{\partial L(\theta,i)}{\partial i}>\mu>0$$

Moreover, consider the fact that the rotor pole arc of the used SRM is larger than its stator pole arc, and the inductance profile does not contain the flatness characteristic. Hence, the coefficient of partial derivative of inductance to position in the produced electromagnetic torque

$$T_e(\theta,i)=\frac{1}{2}\frac{\partial L(\theta,i)}{\partial\theta}i^2$$

is always positive.

Theorem. Consider the uncertain, nonlinear SRM dynamic model (21). The reference speed tracking, without any steady-state error, is ensured by using the control law

$$u=-\frac{1}{g}\left[Ke+\frac{\left(f_0(\mathbf{x},t)-\ddot{\omega}_{ref}\right)^2 e}{\left|\left(f_0(\mathbf{x},t)-\ddot{\omega}_{ref}\right)e\right|+\delta_1\exp\left(-\sigma_1 t\right)}+\frac{\hat{\alpha}^2 e}{|e|\hat{\alpha}+\delta_2\exp\left(-\sigma_2 t\right)}\right], \quad (23)$$

where $K>0$ is the state feedback gain and $e=\dot{\omega}_{ref}-\dot{\omega}$ denotes the error. For notational consistency, the arguments of $f_0(\mathbf{x},t)$ and $g(\mathbf{x},t)$, i.e., $\mathbf{x}$ and t, are omitted during the proof procedures. Exponential parameters δ_1, δ_2, σ_1, σ_2 are some positive constants, selected by the designer, and $\hat{\alpha}$ is the estimation of α, updated by the adaptation mechanism

$$\dot{\hat{\alpha}}=\gamma|e|,\quad \hat{\alpha}(0)=0 \quad (24)$$

where $\gamma>0$ is a positive constant.

Proof. Choosing the Lyapunov function

$$V=\frac{1}{2}e^2+\frac{1}{2}\frac{1}{\gamma}\tilde{\alpha}^2 \quad (25)$$

where $\tilde{\alpha}=\alpha-\hat{\alpha}$ denotes the estimation error. The time derivative of $V$is

$$\dot{V}=e\dot{e}+\frac{1}{\gamma}\tilde{\alpha}\dot{\tilde{\alpha}}=e\dot{e}-\frac{1}{\gamma}\tilde{\alpha}\dot{\hat{\alpha}} \quad (26)$$

By Eq. (21), the error dynamics may be written as

$$\dot{e}=\ddot{\omega}-\ddot{\omega}_{ref}=f_0-\ddot{\omega}_{ref}+h(t)+gu(t) \quad (27)$$

Substituting the error dynamics (27) in (26), one obtains

$$\dot{V}=\left(f_0-\ddot{\omega}_{ref}\right)e+h(t)e+gu(t)e-\frac{1}{\gamma}\tilde{\alpha}\dot{\hat{\alpha}} \quad (28)$$

By assumption 1, $\dot{V}$ is bounded as

$$\dot{V}\le\left|\left(f_0-\ddot{\omega}_{ref}\right)e\right|+\alpha|e|+gu(t)e-\frac{1}{\gamma}\tilde{\alpha}\dot{\hat{\alpha}} \quad (29)$$

Substituting control law (23) in (29) yields

$$\begin{aligned}\dot{V} \le & \left|\left(f_0 - \ddot{\omega}_{ref}\right)e\right| + \alpha|e| - Ke^2 \\ & - \frac{\left(f_0 - \ddot{\omega}_{ref}\right)^2 e^2}{\left|\left(f_0 - \ddot{\omega}_{ref}\right)e\right| + \delta_1 \exp\left(-\sigma_1 t\right)} + \frac{\hat{\alpha}^2 e^2}{|e|\hat{\alpha} + \delta_2 \exp\left(-\sigma_2 t\right)} - \frac{1}{\gamma}\tilde{\alpha}\dot{\hat{\alpha}}\end{aligned} \tag{30}$$

It is straightforward to prove that the inequality $-(p^2/(p+q)) < -p+q$ holds for nonnegative real values p and q where $p^2+q^2 \neq 0$. Hence, manipulating (30) yields

$$\begin{aligned}\dot{V} \le & \left|\left(f_0 - \ddot{\omega}_{ref}\right)e\right| + \alpha|e| - Ke^2 - \left|\left(f_0 - \ddot{\omega}_{ref}\right)e\right| \\ & + \delta_1 \exp\left(-\sigma_1 t\right) - \hat{\alpha}|e| - \delta_2 \exp\left(-\sigma_2 t\right) - \frac{1}{\gamma}\tilde{\alpha}\dot{\hat{\alpha}}\end{aligned} \tag{31}$$

which can be rewritten as

$$\dot{V} \le -Ke^2 + \delta_1 \exp\left(-\sigma_1 t\right) + \delta_2 \exp\left(-\sigma_2 t\right) + (\alpha - \hat{\alpha})|e| - \frac{1}{\gamma}\tilde{\alpha}\dot{\hat{\alpha}} \tag{32}$$

Replacing the update law (24) in (32) gives

$$\dot{V} \le -Ke^2 + \delta_1 \exp\left(-\sigma_1 t\right) + \delta_2 \exp\left(-\sigma_2 t\right) \tag{33}$$

Now, integrating (33) in $0 \le T < \infty$ yields

$$\begin{aligned}V(e(T), \tilde{\alpha}(T)) - V(e(0), \tilde{\alpha}(0)) \le & -K\int_0^T \|e(t)\|^2 \mathrm{d}t + \frac{\delta_1}{\sigma_1}(1 - \exp\left(-\sigma_1 T\right)) \\ & + \frac{\delta_2}{\sigma_2}(1 - \exp\left(-\sigma_2 T\right))\end{aligned} \tag{34}$$

and consequently

$$\begin{aligned}K\int_0^T \|e(t)\|^2 \mathrm{d}t + V(e(T), \tilde{\alpha}(T)) \le & V(e(0), \tilde{\alpha}(0)) + \frac{\delta_1}{\sigma_1}(1 - \exp\left(-\sigma_1 T\right)) \\ & + \frac{\delta_2}{\sigma_2}(1 - \exp\left(-\sigma_2 T\right))\end{aligned} \tag{35}$$

which implies that $\int_0^T \|e(t)\|^2 \mathrm{d}t < \infty$, i.e., $e \in L_2$. On the other hand, by (33), one can conclude

$$\dot{V} \le -Ke^2 + \delta_1 + \delta_2 \tag{36}$$

For any small (near zero) bound $\varepsilon > 0$, the inequality (36) shows that by choosing $K > (\delta_1 + \delta_2)/\varepsilon^2$, there exists a $\kappa > 0$ such that when $|e| > \varepsilon$ the time derivative of Lyapunov function becomes negative, i.e.,

$$\dot{V} \le -\kappa e^2 \le 0 \tag{37}$$

So, the tracking error is bounded, i.e., $e \in L_\infty$. As all of the signals on the right-hand side of error dynamic Eq. (27) is bounded, the boundedness of $\dot{e}$ is ensured, i.e., $\dot{e} \in L_\infty$. Thus, by the Barbalat's lemma [26], the error signal is converged to zero, i.e., $\lim_{t\to\infty} e(t) = 0$. The boundedness of control law can be also concluded by (37).

Remark 1. The exponential terms, formed by δ_1, δ_2, σ_1, and σ_2 in (23), are used to prevent chattering in the control signal. The greater value of such parameters provides the smaller chattering in control signal. On the other hand, there is a trade-off between the smoothness of control effort and the speed of tracking error convergence.

Remark 2. From a theoretical viewpoint, choosing any $K > (\delta_1 + \delta_2)/\varepsilon^2$ ensures holding (37), for any $\varepsilon > 0$, even if K is very large. In practice, selecting an arbitrarily large K may not be possible, and a certain error bound is allowed in controller design.

5. Simulation results

Simulation results are presented here for a SRM with the parameters, given in Appendix B using MATLAB/Simulink. The block diagram of the closed-loop drive control system, using the proposed RASMC, is shown in **Figure 4**. In the following, the system performance is evaluated despite the variation of load torque, as an external disturbance, and compared with that of CASMC. To this end, the CASMC parameters are selected as $K_1 = 20$, $\sigma = 8$, and $\rho = 1$. The RASMC parameters are $K = 10$, $\gamma = 1$ and exponential terms are $\delta_1 = \delta_2 = 5$ and $\sigma_1 = \sigma_2 = 1$. Moreover, the turn-on and turnoff angles are assumed to be constant and equal to 56° and 33°, respectively.

5.1 Tracking performance and disturbance rejection study

To demonstrate the performance of the SRM drive with the proposed control scheme, the load torque is abruptly increased from 5 to 10 Nm at 0.05 sec, as an external disturbance, while the reference speed is 200 rpm. The performance of CASMC and RASMC is compared in **Figure 5**. The chattering phenomenon in control effort is completely removed by the RASMC, as depicted in **Figure 5(b)**.

To demonstrate the effectiveness of using acceleration error in control method, a trapezoidal reference including accelerated part is also used to test the controllers. **Figure 6** shows the response of the system to a four-quadrant trapezoidal reference speed profile. It is shown that the speed response with the proposed RASMC is more precise and smoother than CASMC, obtained by adopting the acceleration closed-loop control.

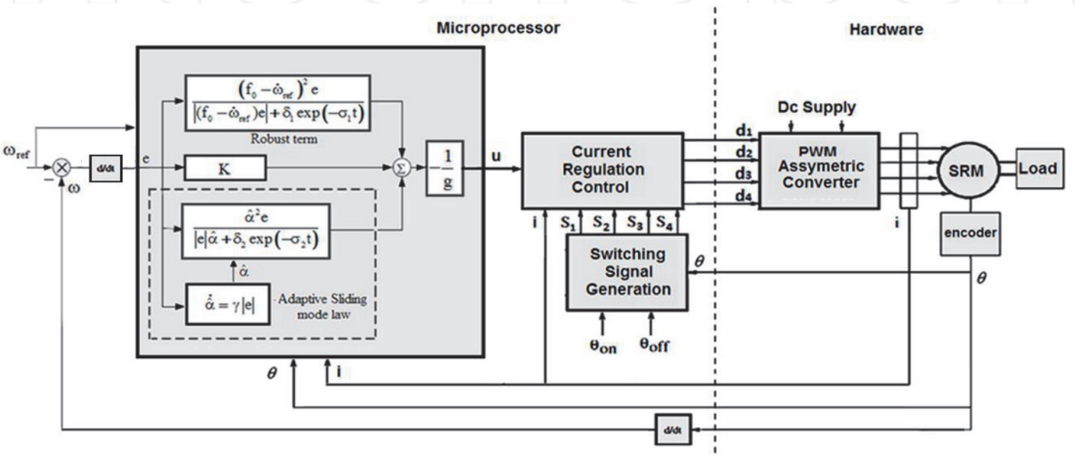


Figure 4.
Overview of the proposed RASMC system for speed control.

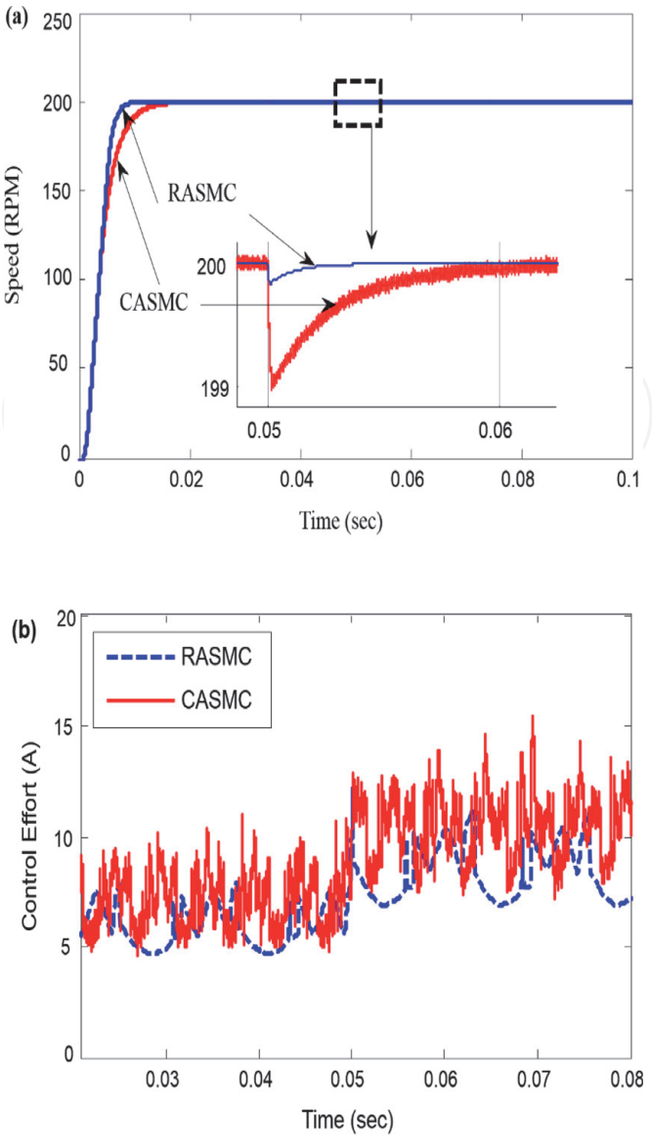


Figure 5.
Performance comparison of controllers, when the motor load increases at 0.05 s from 5 to 10 nm, (a) speed convergence, (b) control effort.

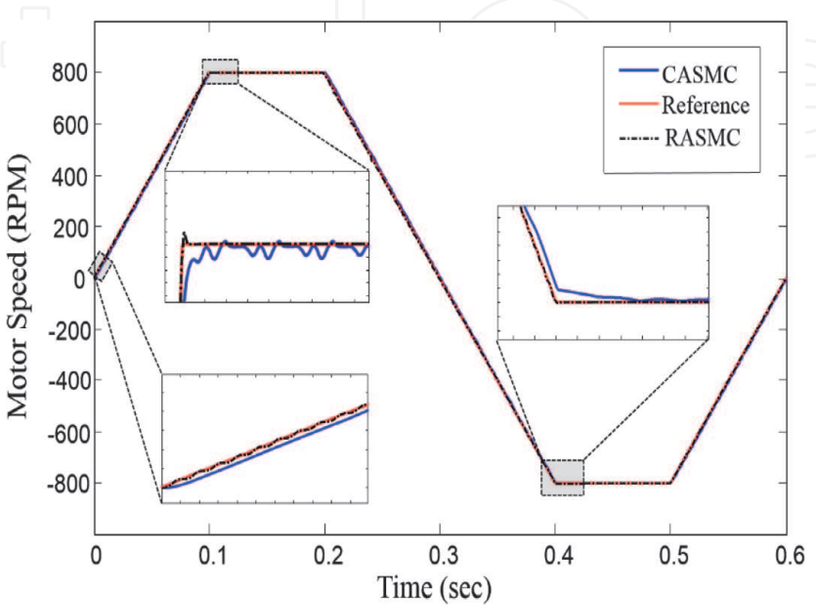


Figure 6.
Four-quadrant speed response of SRM.

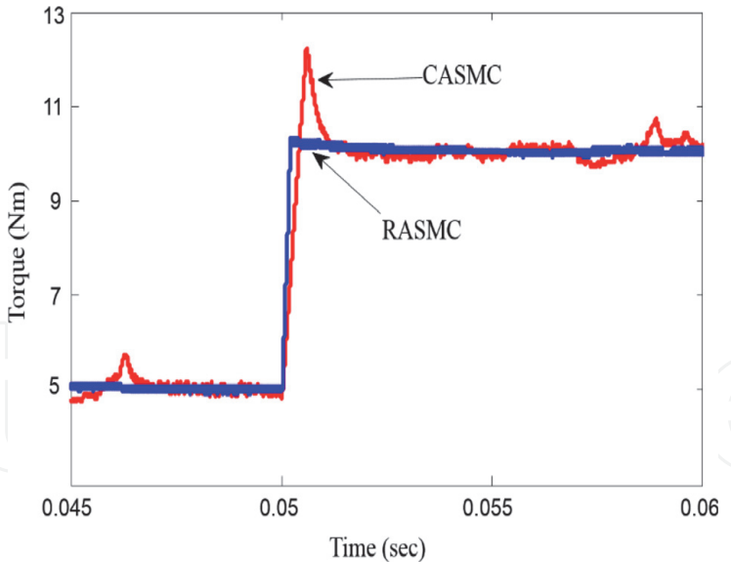


Figure 7.
Performance comparison of the methods in external load disturbance rejection.

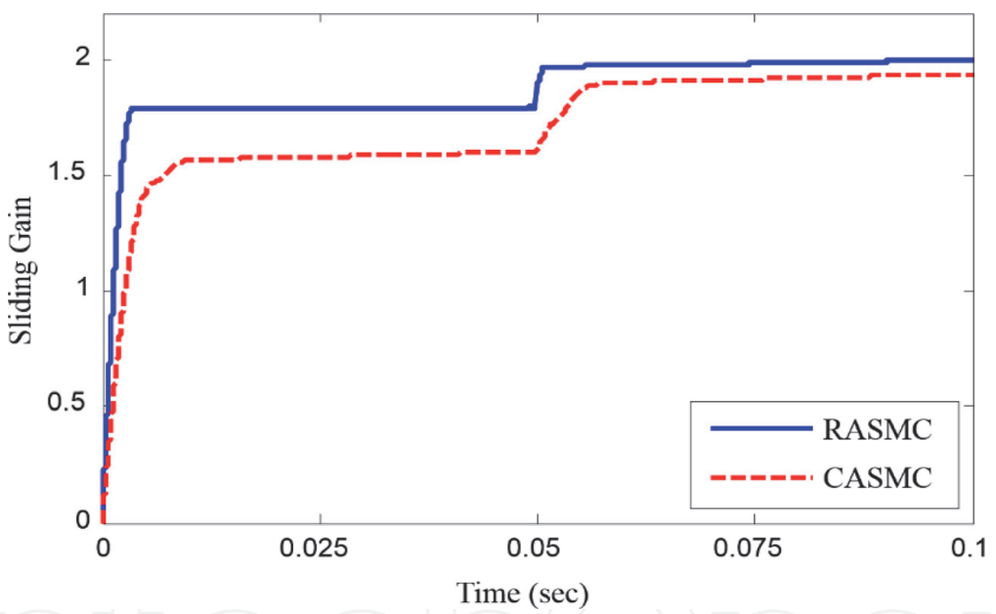


Figure 8.
The sliding gain $\hat{P}$ for CASMC and $\hat{\alpha}$ for RASMC.

The capability of RASMC in external load disturbance rejection, demonstrated in **Figure 7**, shows that a considerable robustness against the external load is achieved, compared with the CASMC. Due to the increased uncertainties of the system caused by the increase in the load torque, there is a speed error at 0.05 sec. **Figure 8** shows the adaptation of the procedure of the proposed adaptive-based controllers, to overcome such system perturbations.

5.2 Robustness against parametric uncertainty

To investigate the behavior of RASMC under parametric variations, the inertia of the motor J, the motor load friction B, and the stator resistance are increased by 100% of the nominal values. Such variations are effectively compensated by the proposed RASMC, as illustrated in **Figure 9**.

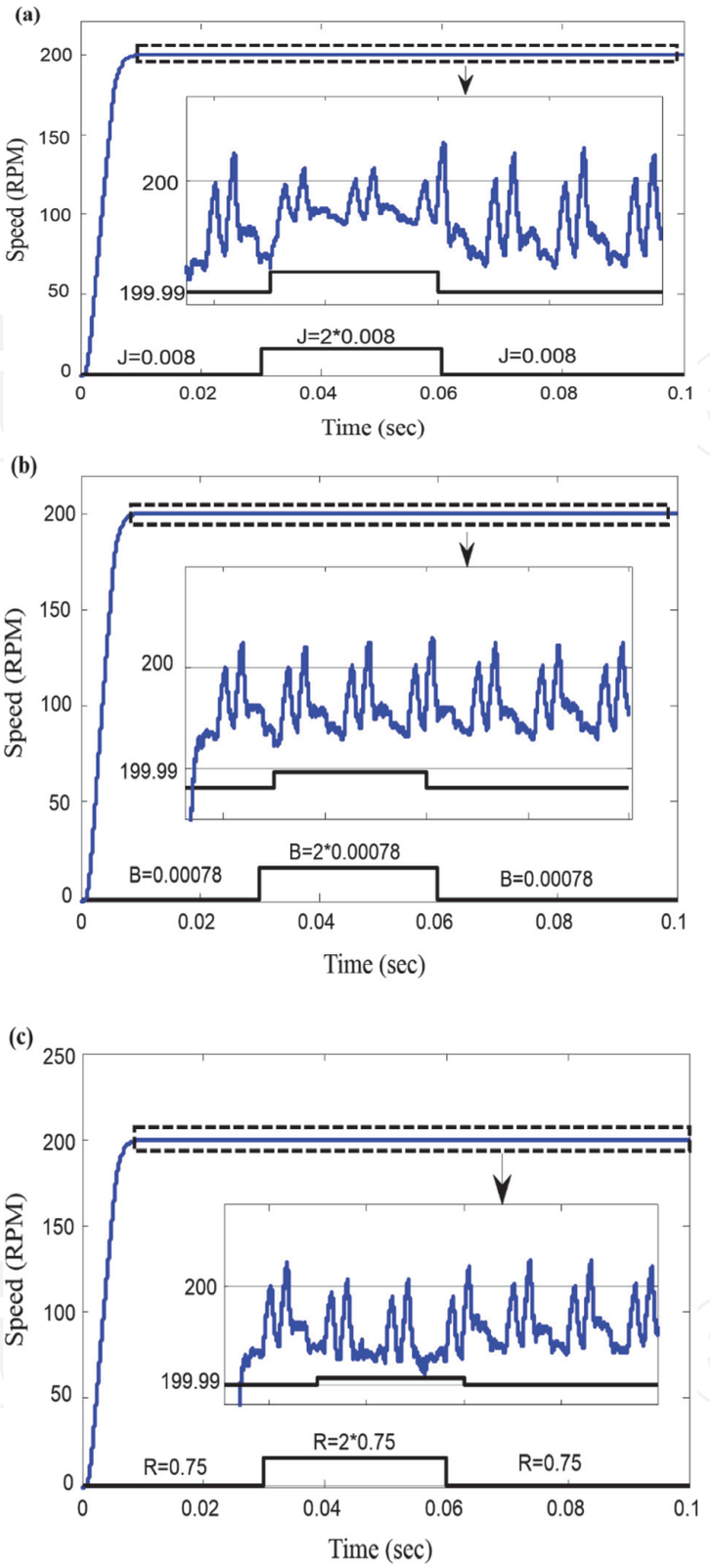


Figure 9.
Speed responses despite the 100% variation in (a) rotational inertia J, (b) viscous friction B, and (c) stator resistance R.

5.3 Rejection of time-varying load perturbations

Applying the load torque with the mean torque values of 10 Nm in 200 RPM and 7 Nm in 500 RPM is shown in **Figures 10** and **11**, respectively. In both cases, the load torque, applied to the motor, is perturbed by a Gaussian noise with variance

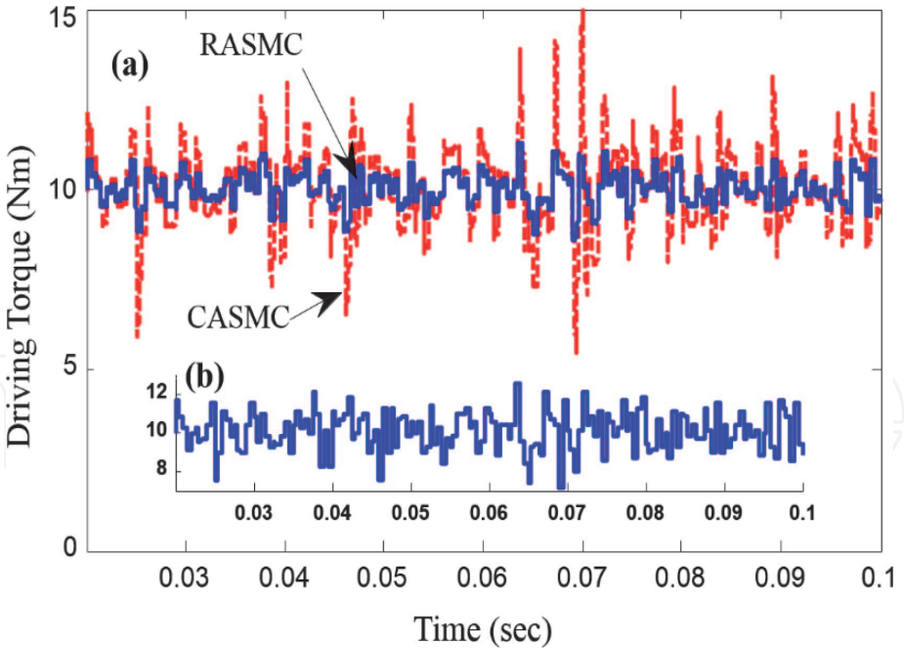


Figure 10.
(a) Torque estimation in the presence of a Gaussian perturbation with a mean of 10 nm and a variance of 1 nm in 200 RPM and (b) applied time-varying load perturbation.

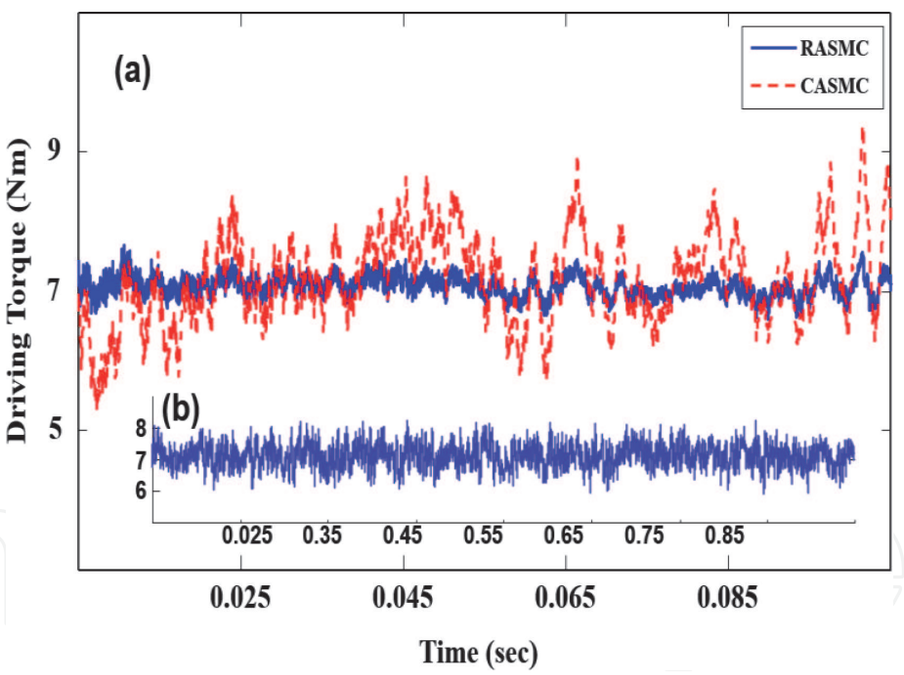


Figure 11.
(a) Torque estimation in the presence of a Gaussian perturbation with a mean of 7 nm and a variance of 1 nm in 500 RPM and (b) applied time-varying load perturbation.

of 1 Nm. These kinds of load torque perturbations are selected to emulate the electric vehicle driving torque condition [30]. The results show only a small ripple remains in the steady state by applying the RASMC.

6. Experimental study

A SRM with same parameters of Appendix B is implemented to experimentally verify the proposed control scheme. The experimental setup is based on a

fixed-point TMS320F2812 DSP, which is compatible with Simulink [31]. Such platform includes four dual pulse-width-modulation (PWM) channels (eight channels total), four analog-to-digital converters (ADCs), and a speed encoder input.

Figures 12 and **13** illustrate the laboratory setup and the general layout of the DSP-based drive system, respectively. The experimental hardware, used for evaluating the 8/6 SRM drive, consists of the following sections:

(i) The asymmetrical converter, implemented by using IXSH 35N120A IGBT with a gate driver TLP250 and fast power diodes DSEI 20-12A with a reverse recovery time, less than 40 nanoseconds. (ii) Hall-type galvanic isolation CSNE151–104 Honeywell sensors for measuring the phase currents. A ten-bit absolute encoder Autonics EP50S8, used to determine the rotor position with high accuracy. (iii) The results are obtained under the speed loop switching frequency of 10 kHz and the current loop of 1 kHz. The DC link voltage is kept constant at 280 V.

Some experimental results are presented here by implementing the RASMC and CASMC, from a comparison viewpoint. The numerical values of the parameters,

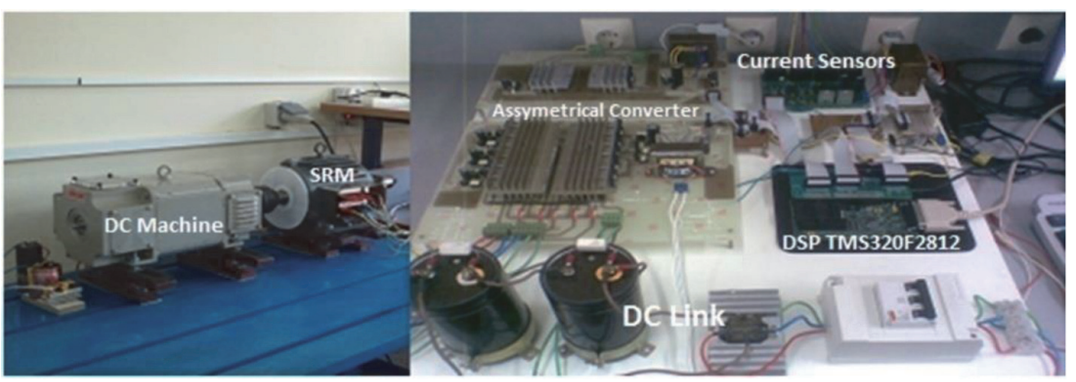


Figure 12.
The laboratory setup for experimental study.

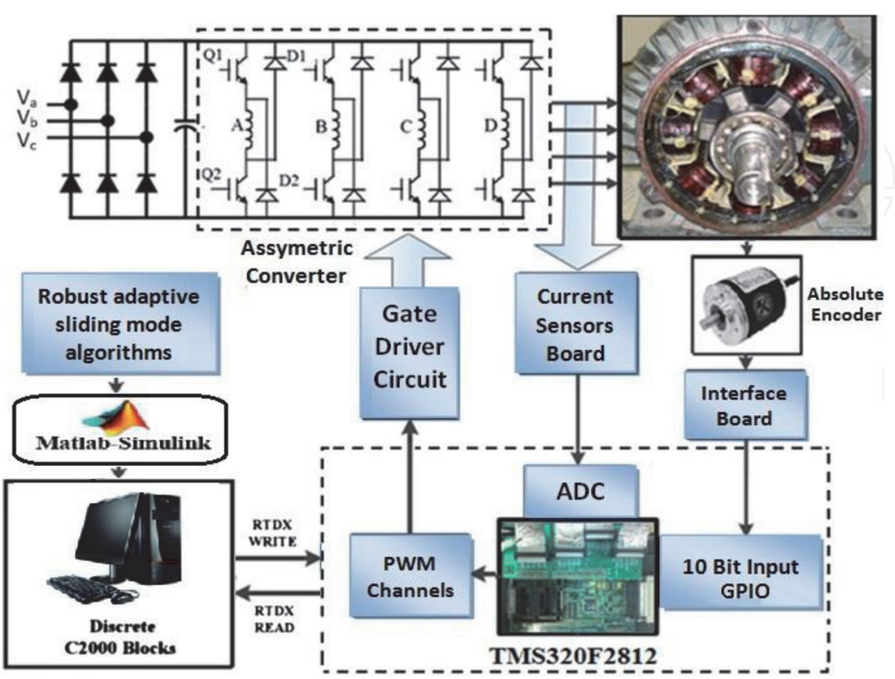


Figure 13.
Block diagram of the experimental platform.

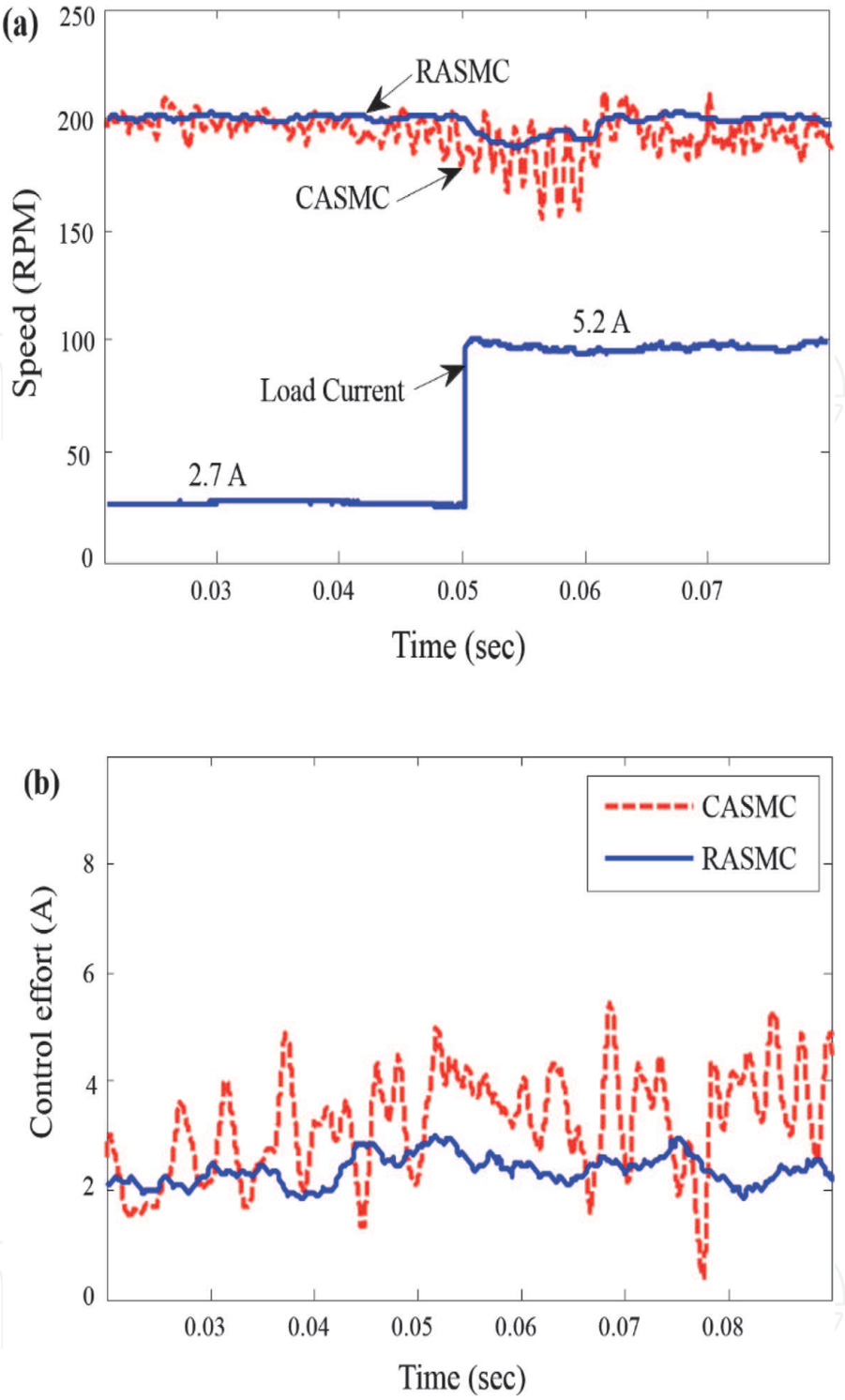


Figure 14.
Performance of the proposed RASMC in experiment under abrupt load change, compared with that of CASMC (a) speed response and load current and (b) control effort.

obtained in the simulation studies by trial and error, are used here in the experimental investigations. **Figures 14(a)** and **15(a)** demonstrate the speed response, respectively, under an abrupt external load change from 5 to 10 Nm at 0.05 sec and under a step change in the reference speed from 100 to 200 RPM. Since a torque sensor was not available, for the electromagnetic torque, only armature current of DC generator as a load is depicted in **Figure 14(a)**. Stepping the armature current

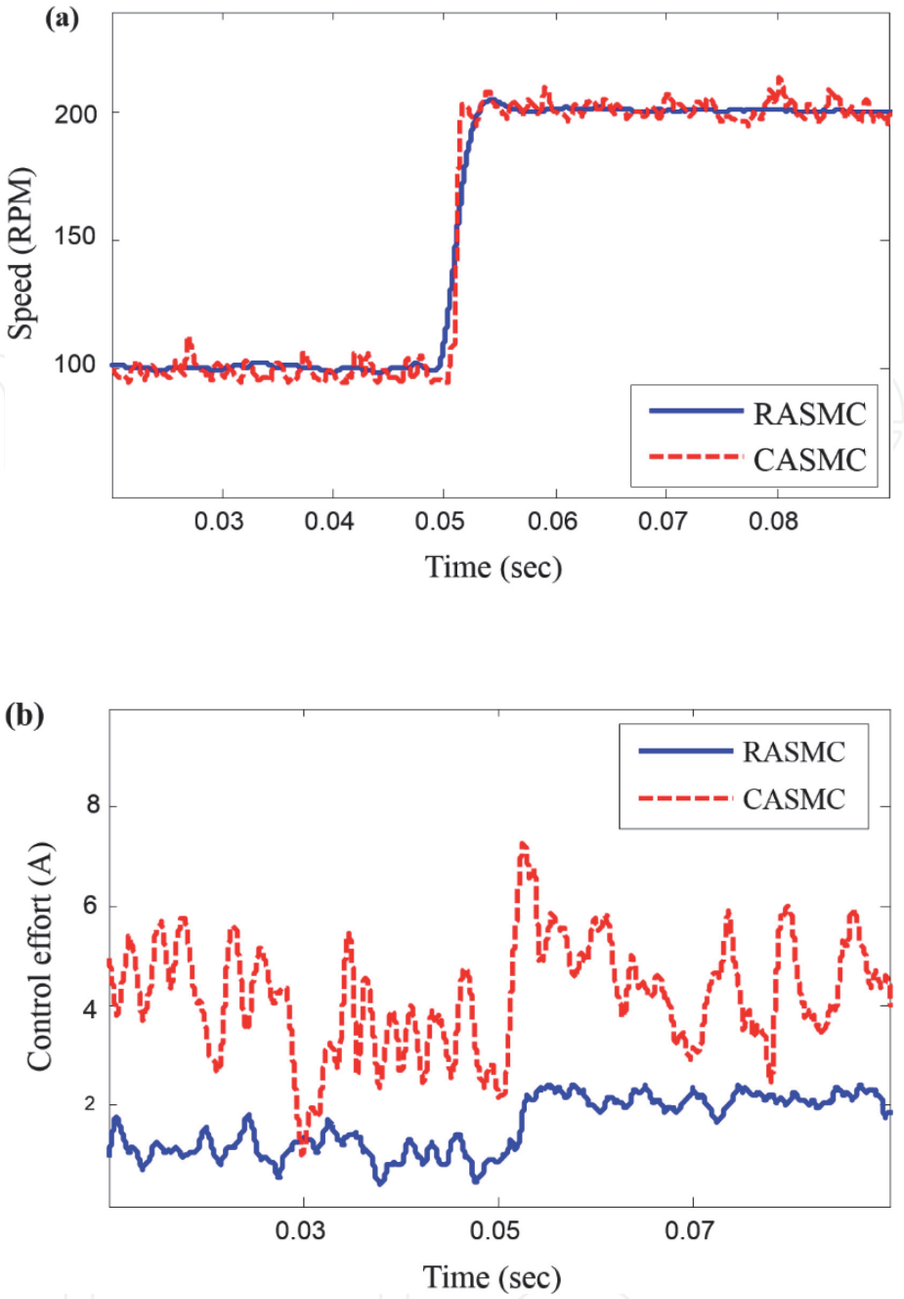


Figure 15.
Performance of the RASMC in experiment, under step increment of reference speed, compared with that of CASMC (a) speed response in steady state and (b) control effort.

from 2.7 to 5.2 A is equal to stepping load torque from 5 to 10 Nm. The results show that the RASMC significantly improves the robustness performance. As expected, the RASMC successfully eliminates the chattering in the control efforts, as shown in **Figures 14(b)** and **15(b)**. By comparing the results of experimental work with those of the simulation study, the demonstration in **Figure 5** is confirmed. Briefly discussing, the results of implementing RASMC not only confirm the better performance in smoothing the control effort but also demonstrate the disturbance attenuation property. As a confirmatory data, **Figure 16(a)** and **(b)** depicts the waveforms of experimental current and voltage of two phases for CASMC and RASMC, respectively. It is obvious that the current and voltage signals are smoother by using the RASMC.

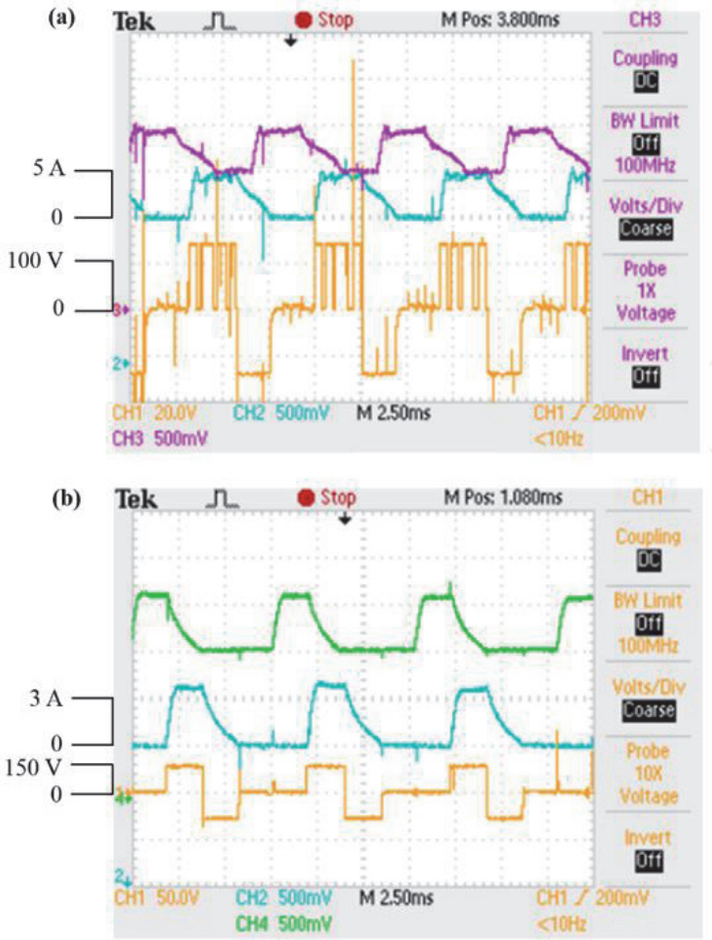


Figure 16.
Two phase currents and voltages for (a) CASMC and (b) RASMC.

7. Conclusion

Two nonlinear adaptive sliding mode control algorithms are developed for speed control of SRM in the application of EVs, especially in urban areas that the speed is low and the driving torque is highly fluctuated. This condition is emulated by applying a Gaussian noise to perturb the load torque. First, a conventional adaptive sliding mode control is designed to yield a chattering-free control algorithm. However, linearized SRM model is used, and only mechanical uncertainty of SRM dynamic model is considered.

To implement a high-performance control algorithm for removing these drawbacks, a robust adaptive sliding mode control, namely, RASMC, is proposed. An augmented time-varying uncertainty is defined taking into account the SRM full nonlinear dynamic model and the system uncertainties as well as time-varying load perturbation.

The upper bound of defined augmented uncertainty is not required to be known to make the control gain small enough in order to decrease the chattering and efforts of the controller. Moreover, the exponential terms in sliding function are used to prevent chattering in the control signal. The proposed controller is capable of achieving torque ripple minimization with reduced smooth control effort. The simulation and experimental results also confirm the robustness properties against model uncertainties and time-varying load torque disturbances with significant improvement in speed control loop transient response.

Appendix A. Derivation of Eq. (9) in detail

As stated in Section 3, the Lyapunov function is defined in (8) as

$$V = \frac{1}{2}S^2 + \frac{1}{2\rho}\tilde{P}^2 \rightarrow \dot{V} = S\dot{S} + \frac{1}{\rho}\tilde{P}\dot{\tilde{P}} \tag{A.1}$$

where $\tilde{P} = P - \hat{P}$ and $P = \frac{1}{b}\left(\dot{\omega}\Delta a + \Delta b\left(\dot{T}_e - \dot{T}_L\right)\right)$ defined from (5) are assumed to be constant during the sampling period. Hence, it can be concluded that $\dot{\tilde{P}} = -\dot{\hat{P}}$. By substituting (7) into (A.1), and adding and subtracting K_1S^2, the derivative of Lyapunov function can be written as

$$\dot{V} = S\dot{S} - \frac{1}{\rho}\tilde{P}\dot{\hat{P}} = -K_1S^2 + K_1S^2 + S\left[-(\sigma + a)\dot{\omega} - bu + b\dot{T}_{\mathrm{L}} - b\left(\tilde{P} + \hat{P}\right)\right] - \frac{1}{\rho}\tilde{P}\dot{\hat{P}} \tag{A.2}$$

Finally it can be simplified as

$$\dot{V} = \ -K_1S^2 + S\left[-(\sigma + a)\dot{\omega} - b\left(u + \hat{P}\right) + b\dot{T}_{\mathrm{L}} + K_1S\right] - \tilde{P}\left(\frac{1}{\rho}\dot{\hat{P}} + bS\right) \tag{A.3}$$

B. Numerical values of the SRM parameters

Parameters	Value
Rated power	4 kW
RMS rated phase current	9 A
Rated DC link	280 V
Number of poles	8/6
Phase stator resistance	0.75 Ω
Rotational inertia (J)	0.008 Nms^2
Viscous friction (B)	0.00078 Nms
Aligned inductance	0.114 mH
Unaligned inductance	0.0136 mH

IntechOpen

IntechOpen

Author details

Mohammad Masoud Namazi[1*], Hamid Reza Koofigar[1] and Jin-Woo Ahn[2]

1 Department of Electrical Engineering, University of Isfahan, Isfahan, Iran

2 Department of Mechatronics Engineering, Kyungsung University, Busan, South Korea

*Address all correspondence to: m.namazi@eng.ui.ac.ir

IntechOpen

© 2020 The Author(s). Licensee IntechOpen. This chapter is distributed under the terms of the Creative Commons Attribution License (http://creativecommons.org/licenses/by/3.0), which permits unrestricted use, distribution, and reproduction in any medium, provided the original work is properly cited. CC BY

References

[1] Krishnan R. Switched Reluctance Motor Drives. Boca Raton, FL: CRC Press; 2001

[2] Li B, Ling X, Huang Y, Gong L, Liu C. Predictive current control of a switched reluctance machine in the direct-drive manipulator of cloud robotics. Cluster Computing. 2017;**20**(4):3037-3049. DOI: 10.1007/s10586-017-0983-4

[3] Tseng CL, Wang SY, Chien SC, Chang CY. Development of a self-tuning TSK-fuzzy speed control strategy for switched reluctance motor. IEEE Transactions on Power Electronics. 2012;**27**:2141-2152

[4] Al-Mayyahi A, Ali RS, Thejel RH. Designing driving and control circuits of four-phase variable reluctance stepper motor using fuzzy logic control. Electrical Engineering. June 2018; **100**(2):695-709

[5] Sahoo SK, Dasgupta S, Panda SK, Xu JX. A Lyapunov function-based robust direct torque controller for a switched reluctance motor drive system. IEEE Transactions on Power Electronics. 2012;**27**:555-564

[6] Rigatos G, Siano P, Ademi S. Nonlinear H-infinity control for switched reluctance machines. Nonlinear Engineering. 2020;**9**:14-27

[7] Rajendran A, Padma S. H-infinity robust control technique for controlling the speed of switched reluctance motor. Frontiers of Electrical and Electronic Engineering. 2012;**7**:337-346

[8] Loría A, Espinosa-Pérez G, Chumacero E. Robust passivity-based control of switched-reluctance motors. International Journal of Robust and Nonlinear Control. 2015;**25**:3384-3403

[9] Chumacero E, Loría A, Espinosa-Pérez G. Robust adaptive control of switched-reluctance motors without velocity measurements. In: 2013 European Control Conference (ECC), Zurich. 2013. pp. 4586-4591

[10] Loria A, Espinosa-Perez G, Chumacero E. Exponential stabilization of switched-reluctance motors via speed-sensorless feedback. IEEE Transactions on Control Systems Technology. May 2014;**22**(3): 1224-1232

[11] Bizkevelci E, Leblebicioglu K, Ertan HB. A sliding mode controller to minimize SRM torque ripple and noise. In: IEEE International Symposium on Industrial Electronics, vol. 2. 2004. pp. 1333-1338

[12] Sahoo SK, Panda SK, Xu JX. Direct torque controller for switched reluctance motor drive using sliding mode control. In: IEEE International Conference on Power Electronics and Drives Systems, vol. 2. 2005. pp. 1129-1134

[13] Alrifai M, Zribi M, Rayan M, Krishnan R. Speed control of switched reluctance motors taking into account mutual inductances and magnetic saturation effects. Energy Conversion and Management. 2010;**51**:1287-1297

[14] Ro HS, Jeong HG, Lee KB. Torque ripple minimization of switched reluctance motor using direct torque control based on sliding mode control. In: International Symposium on Industrial Electronic, Taiwan. 2013

[15] Namazi MM, Borujeni MM, Rashidi A, Nejad SMS, Ahn J. Torque ripple reduction of switched reluctance motor drive with adaptive sliding mode control and particle swarm optimization. In: 2015 IEEE International Conference on Advanced Intelligent Mechatronics (AIM), Busan. 2015. pp. 371-376

[16] Shang W, Zhao S, Shen Y, Qi Z. A sliding mode flux-linkage controller with integral compensation for switched reluctance motor. IEEE Transactions on Magnetics. 2009;**45**:3322-3328

[17] Perruquetti W, Barbot JP. Sliding Mode Control in Engineering. Marcel Dekker; 2002

[18] Wang S-Y, Liu F-Y, Chou J-H. Adaptive TSK fuzzy sliding mode control design for switched reluctance motor DTC drive systems with torque sensorless strategy. Applied Soft Computing. 2018;**66**:278-291

[19] Azadru A, Masoudi S, Ghanizadeh R, Alemi P. New adaptive fuzzy sliding mode scheme for speed control of linear switched reluctance motor. IET Electric Power Applications. 2019;**13**(8):1141-1149

[20] Hu K, Ye J, Velni JM, Guo L, Yang B. A fixed-switching-frequency sliding mode current controller for mutually coupled switched reluctance machines using asymmetric bridge converter. In: 2019 IEEE Transportation Electrification Conference and Expo (ITEC), Detroit, MI, USA. 2019. pp. 1-6

[21] Lin CK, Liu TH, Wei MY, Fu LC, Hsiao CF. Design and implementation of a chattering-free nonlinear sliding-mode controller for interior permanent magnet synchronous drive systems. IET Electric Power Applications. 2012;**6**: 332-344

[22] Ling R, Wu M, Dong Y, Chai Y. High order sliding-mode control for uncertain nonlinear systems with relative degree three. Communications in Nonlinear Science and Numerical Simulation. 2012;**17**:3406-3416

[23] Mondal S, Mahanta C. Nonlinear sliding surface based second order sliding mode controller for uncertain linear systems. Communications in Nonlinear Science and Numerical Simulation. 2011;**16**:3760-3769

[24] Rafiq M, Rehman S, Rehman F, Butt QR, Awan I. A second order sliding mode control design of a switched reluctance motor using super twisting algorithm. Simulation Modelling Practice and Theory. 2012;**25**:106-117

[25] Rain X, Hilairet M, Talj R. Second order sliding mode current controller for the switched reluctance machine. In: IEEE 36th Annual Conference on Industrial Electronics Society, IECON. 2010. pp. 3301-3306

[26] Noroozi N, Roopaei M, Jahromi MZ. Adaptive fuzzy sliding mode control scheme for uncertain systems. Communications in Nonlinear Science and Numerical Simulation. 2009;**14**: 3978-3992

[27] Huang YJ, Kuo TC, Chang SH. Adaptive sliding mode control for nonlinear systems with uncertain parameters. IEEE Transactions on Systems, Man, and Cybernetics, Part B: Cybernetics. 2008;**38**:534-539

[28] Faieghi MR, Delavari H, Baleanu D. A novel adaptive controller for two-degree of freedom polar robot with unknown perturbations. Communications in Nonlinear Science and Numerical Simulation. 2012;**17**: 1021-1030

[29] Barambones O, Garrido AJ. Adaptive sensorless robust control of AC drives based on sliding mode control theory. International Journal of Robust and Nonlinear Control. 2007;**17**: 862-879

[30] Pupadubsin R, Chayopitak N, Taylor DG, Nulek N, Kachapornkul S, Jitkreeyarn P, et al. Adaptive integral sliding-mode position control of a coupled-phase linear variable reluctance motor for high-precision applications.

IEEE Transactions on Industry Applications. 2012;**48**:1352-1363

[31] Shtessel Y, Taleb M, Plestan F. A novel adaptive-gain supertwisting sliding mode controller: Methodology and application. Automatica. 2012;**48**: 759-769

[32] Mondal S, Mahanta C. A fast converging robust controller using adaptive second order sliding mode. ISA Transactions. 2012;**51**:713-721

[33] Namazi Isfahani MM, Rashidi A, Saghaian-Nejad SM. Energy-based adaptive sliding mode speed control for switched reluctance motor drive systems. Iranian Journal of Electrical & Electronic Engineering. Mar. 2012;**8**(1): 68-75

[34] Namazi MM, Rashidi A, Saghaian-Nejad SM, Ahn J-W. Chattering-free robust adaptive sliding-mode control for switched reluctance motor drive. In: 2016 IEEE Transportation Electrification Conference and Expo, Asia-Pacific (ITEC Asia-Pacific), Busan. 2016. pp. 474-478

[35] Namazi Isfahani MM, Saghaian-Nejad SM, Rashidi A, Abootorabi Zarchi H. Passivity-based adaptive sliding mode speed control of switched reluctance motor drive considering torque ripple reduction. In: 2011 IEEE International Electric Machines & Drives Conference (IEMDC), Niagara Falls, ON. 2011. pp. 1480-1485

[36] Koofigar HR, Hosseinnia S, Sheikholeslam F. Robust adaptive nonlinear control for uncertain control-affine systems and its applications. Nonlinear Dynamics. 2009;**56**:13-22

[37] Namazi MM, Rashidi A, Koofigar H, Saghaiannejad SM, Ahn JW. Adaptive control of switched reluctance motor drives under variable torque applications. Journal of Electrical Engineering and Technology. 2017; **12**(1):134-144